

Grating-based holographic diffraction methods for X-rays and neutrons: phase object approximation and dynamical theory

Hao Feng,^{a,b,*} Rana Ashkar,^c Nina Steinke,^d Robert Dalglish,^d Nickolay V. Lavrik,^e Ivan I. Kravchenko^e and Roger Pynn^{a,b,f}

Received 14 June 2017
Accepted 22 November 2017

Edited by G. J. McIntyre, Australian Centre for Neutron Scattering, Australia

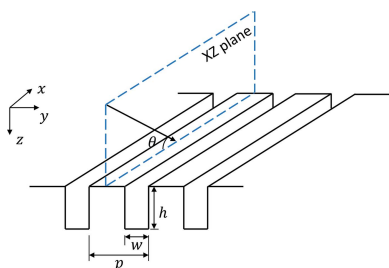
Keywords: grating-based holography; phase object approximation; dynamical theory.

^aCenter for Exploration of Energy and Matter, Indiana University, Bloomington, IN 47408, USA, ^bPhysics Department, Indiana University, Bloomington, IN 47405, USA, ^cBiology and Soft Matter Division, Oak Ridge National Laboratory, Oak Ridge, TN 37831, USA, ^dISIS Facility, Rutherford Appleton Laboratory, Chilton, Oxfordshire OX11 0QX, UK, ^eCenter for Nanophase Materials Science, Oak Ridge National Laboratory, Oak Ridge, TN 37831, USA, and ^fNeutron Sciences Directorate, Oak Ridge National Laboratory, Oak Ridge, TN 37831, USA. *Correspondence e-mail: fenghao@indiana.edu

A method dubbed grating-based holography was recently used to determine the structure of colloidal fluids in the rectangular grooves of a diffraction grating from X-ray scattering measurements. Similar grating-based measurements have also been recently made with neutrons using a technique called spin-echo small-angle neutron scattering. The analysis of the X-ray diffraction data was done using an approximation that treats the X-ray phase change caused by the colloidal structure as a small perturbation to the overall phase pattern generated by the grating. In this paper, the adequacy of this weak phase approximation is explored for both X-ray and neutron grating holography. It is found that there are several approximations hidden within the weak phase approximation that can lead to incorrect conclusions from experiments. In particular, the phase contrast for the empty grating is a critical parameter. While the approximation is found to be perfectly adequate for X-ray grating holography experiments performed to date, it cannot be applied to similar neutron experiments because the latter technique requires much deeper grating channels.

1. Introduction

Confined colloidal fluids are important in modern technologies such as interfacial adhesion, lubrication and the flow of drugs through narrow channels (Daw & Finkelstein, 2006; Windbergs & Weitz, 2011). To understand the colloidal behavior in such complex systems, the study of model colloids under confinement is essential. While the arrangement of micrometre-sized colloidal particles in confinement can be studied using various forms of microscopy, small submicrometre-scale particles are harder to probe. Recently, a group at the Paul Scherrer Institute (PSI) developed a technique which they dubbed X-ray grating holography to study the structures adopted by small colloidal particles confined between parallel walls (Bunk *et al.*, 2007; Nygård *et al.*, 2008, 2009; Satapathy *et al.*, 2009). The method uses a diffraction grating with regularly spaced rectangular grooves (Fig. 1) in contact with a bulk colloidal suspension. The walls of the grooves serve to confine the colloidal particles within the grooves. Since the grating periodicity is of the order of one micrometre, *i.e.* several times smaller than the beam size, colloidal particles in many grooves contribute to the scattering, thus enhancing the scattered signal. Moreover, the periodic arrangement of the grooves causes the scattering to appear at well defined Bragg peaks.



Using this method, the PSI group explored several colloidal systems with different particle sizes, groove widths and pH of the solvent. They found that, depending on the ratio of groove width to effective particle size, the colloids can assemble into layers parallel to the groove walls or undergo what they called a buckling instability (Bunk *et al.*, 2007; Nygård *et al.*, 2009; Satapathy *et al.*, 2009).

Noting that neutron scattering contrast between colloidal particles and a solvent can often be enhanced by selective deuteration, we used a similar colloidal suspension in deuterated solvent to test the efficacy of neutron scattering in probing the same colloidal phenomena (Ashkar *et al.*, 2014). Demonstrating such efficacy is important because, in the future, one can imagine using neutron grating holography methods to probe the effects of confinement on other materials, such as block copolymers, for which neutron scattering has proved to be an important tool. The fact that the X-ray experiments indicated that the colloids in the grooves have the same volume fraction as the bulk (Nygård *et al.*, 2009) also provided an impetus for our neutron experiments. It was important to explore whether this was a mere artifact of the bulk concentration that they chose, which is quite close to what one would expect in a layered close-packed colloidal assembly, or if it applies to suspensions of different concentrations. However, because neutron sources are much weaker than X-ray synchrotrons, conventional neutron diffractometers cannot resolve multiple orders of Bragg peaks from structures with micrometre-scale periodicity as X-rays do. We thus resorted to a relatively new method called spin-echo small-angle neutron scattering (SESANS), which does have sufficient resolution for this type of system (Gähler *et al.*, 1996; Rekveldt, 1996; Rekveldt *et al.*, 2005). In our first neutron grating holography experiments we could not confirm particle layering within the measured statistics, but we observed that the colloidal volume fraction in the grooves was significantly

greater than that in the bulk suspension above the grooves (Ashkar *et al.*, 2014).

We analyzed our neutron holography data using a dynamical theory (DT) that had been shown to give a very good account of SESANS data obtained with empty diffraction gratings both in transmission and in reflection geometries (Ashkar *et al.*, 2011). This method differs from the one used by the PSI group, which is based on the phase object approximation (POA) and on a perturbation theory that treats the modification of the scattering caused by colloidal structure as a weak effect. Given the difference in the conclusions from the X-ray and neutron experiments it is natural to ask whether these differences could arise from the methods of analysis. A further motivation arises because the X-ray analysis provides a very simple way of obtaining the colloid structure from the Patterson function of the scattering. We note that the Patterson functions for X-ray holography are obtained in a standard manner from the measured Bragg intensities. However, since SESANS measures the Patterson function directly, the question arises as to whether the analysis method used to treat X-ray holography can be applied to SESANS grating holography, substantially simplifying the method by obviating the need for a complex DT calculation. This report attempts to answer that question.

Both the DT and the POA have been applied to SESANS data obtained with diffraction gratings in transmission. For the published cases (Haan *et al.*, 2007; Ashkar *et al.*, 2011), both methods describe SESANS data well and they provide results that are almost indistinguishable from one another. Nevertheless, using the DT code presented by Ashkar *et al.* (2010), it is easy to show that the DT and the POA do not give the same Bragg intensities and that the agreement between theory and the SESANS results has to be viewed with caution. Because the SESANS signal is, in fact, identical to the Patterson function of the grating with the zeroth-order Bragg scattering included, it is the result of summing a large number of Bragg intensities multiplied by the appropriate cosine functions (Ashkar *et al.*, 2010). In this framework, it is important to point out that (a) positive and negative differences between the Bragg intensities predicted by the POA and the DT tend to cancel one another in the Patterson function, and (b) it is often the case that the first few Bragg peaks make dominant contributions to the Patterson function, and these peaks may have similar intensities in both the POA and the DT. Thus, the differences between the Patterson functions predicted by the POA and the DT are often small and easy to overlook when comparing these theories with experimental results for scattering from a particular grating. However, the method of analysis used by X-ray grating holography relies entirely on the difference between a measured Patterson function and one calculated assuming that the POA is valid. This difference, which is supposed to represent the scattering due to colloidal structure (such as layering), is, by definition, very small. Thus, a small error in a calculated Patterson function could have a large effect on the analysis because it could be significant in relation to the scattering caused by colloidal structure. For a grating with a truly rectangular profile (which we treat here),

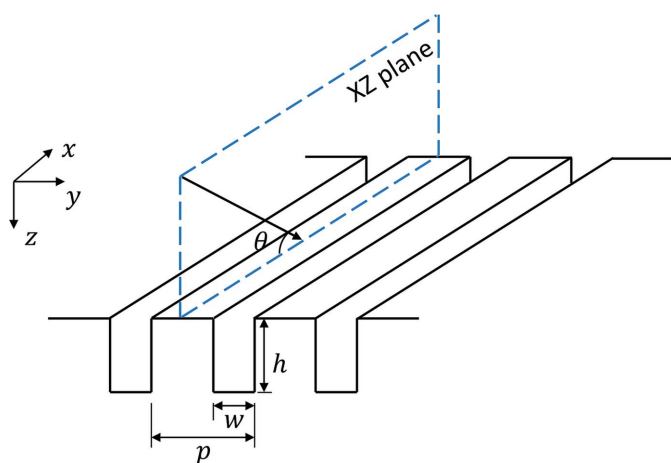


Figure 1 Schematic of the rectangular grating profile with grating period p , groove width w and groove depth h . The incident X-ray or neutron beam is in the xz plane and forms an angle θ with respect to the grating surface. Parameters for the gratings used in neutron and X-ray experiments are given in Table 1.

we expect that the DT and the POA must eventually disagree with one another as the grating grooves are made deeper. At some depth, the phase difference between X-ray or neutron waves passing through the grooves and walls of the grating reaches 2π . At this value, the POA predicts no scattering, because there is no spatial variation of the scattering phase, whereas the DT does not give that answer. Our calculations for rectangular gratings indicate that clear differences between the Patterson functions predicted by the POA and the DT arise for phase differences greater than about π , and the gratings used for neutron holography fall into this category.

It will become clear, as we go through the analysis, that there are other reasons to question whether the POA is a good approximation to use for the analysis of grating holography but, for the moment, the above paragraph is a sufficient motivation for using the DT in the calculations reported here. We believe that the DT gives the correct result for scattering from gratings, not only because it has adequately described all experiments analyzed to date but also because it includes essential physics such as multiple scattering and energy conservation that are not addressed by the POA. Accordingly, we use the DT in this paper to simulate scattering intensities for two gratings that have been used for X-ray and neutron experiments performed to date. The simulations include layering of the colloidal particles within the grooves. We then use the X-ray analysis method to retrieve the scattering profile of a structured colloid from the DT ‘data’ and compare it with the profile used as input to the DT calculations. The two gratings that we discuss in this paper are those used in the X-ray holography paper (Nygård *et al.*, 2009) and a neutron paper that will be published shortly. These gratings are both very close to perfectly rectangular and this is the shape assumed here, although we will comment on the effects of sloping channel walls towards the end of this report. While the periods of the gratings are similar and the material used (silicon) is the same, the effective depths of the grating grooves are different: $\sim 2.4\ \mu\text{m}$ for X-rays and $\sim 53\ \mu\text{m}$ for neutrons.

The reason for the different depths of the X-ray and neutron gratings has to do with the fact that the X-ray and neutron methods employ different Patterson functions. In the X-ray case, the Patterson function is computed by summing all non-zeroth-order Bragg peaks multiplied by the appropriate cosine factors (Nygård *et al.*, 2009). SESANS, on the other hand, measures a Patterson function that includes the zeroth-order Bragg peak (Krouglov *et al.*, 2003). This means that small changes in Bragg peak intensities, due for example to colloidal arrangement in the grooves, produce much smaller fractional changes in the SESANS signal than in the Patterson function computed in the X-ray case. To compensate for this effect, the effective depth of the neutron holography grating has to be much larger than the X-ray grating.

This paper is organized as follows: first, the approximations involved in the weak phase analysis of the X-ray holography method are briefly reviewed. Then, the two types of gratings with rectangular profiles used in this paper are introduced.

Next, the approximations applied in the X-ray holography method are investigated and the results of applying the X-ray analysis method to the two gratings are presented. Finally, we discuss the essential lessons we have learned and comment on the effect of trapezoidal grating profiles.

2. Approximations used to analyze X-ray grating holography

The usual POA postulates that a scattering object changes only the phase of a forward-scattered wave passing through it (Jap & Glaeser, 1978; Haan *et al.*, 2007). For X-rays or neutrons, the difference in phase between a wave propagating in vacuum and one traversing a path of the same length through a scattering object depends on the radiation wavelength and the scattering length density (SLD) integrated along the path through the object. The SLDs are related to the real part of the refractive index, $1 - \delta$, normally used for X-rays by $\rho = 2\pi\delta/\lambda^2$, where ρ is the SLD and λ the wavelength of the radiation. For grating holography, we write the X-ray or neutron phase, relative to the phase accumulated through the grating walls, as a function of the position, y , across the grating (*cf.* Fig. 1) as $\Delta\varphi(y) = \overline{\Delta\varphi}f(y) + \omega(y)$. Here, $\overline{\Delta\varphi}$ is the phase difference between the phase accumulated through the average colloid and that through the grating wall, where average colloid refers to the homogeneous medium whose optical path length is the same as the coarse-grained average of the colloidal suspension; $f(y)$ is a step function with value 1 inside a groove and 0 elsewhere; $\omega(y)$ is the phase change, relative to that of the homogeneous colloid, due to non-random distribution (*e.g.* layering) of the colloids within the grating channels. In this report, we use ‘homogeneously filled grating’ to refer to a grating filled with the average colloid.

The method introduced by Nygård *et al.* (2009) for the analysis of X-ray grating holography is based on two key assumptions. The first is that scattering from the homogeneously filled grating can be estimated by multiplying the measured Bragg intensities for the empty grating by a constant that is independent of Bragg order. This assumption is strictly correct only for a system whose SLD modulation has a rectangular profile and whose scattering can be described by the POA or by a kinematic theory (Diaz & van der Veen, 2007). It is not, in general, correct for the DT although it sometimes gives results that are numerically quite close to those obtained from the POA, especially for shallow gratings. The second approximation is that $\exp[i\Delta\varphi(y)]$ can be expanded adequately to first order as $\exp[i\overline{\Delta\varphi}f(y)][1 + i\omega(y)]$. With these two approximations, the modulation of the SLD due to colloidal structure in the grooves can be written as a simple linear equation that is directly solvable (see Appendix A).

3. Gratings used in X-ray and SESANS experiments

The X-ray and neutron simulations discussed here both use diffraction gratings with a rectangular profile, as shown in

Table 1
Parameters for the gratings and colloids used in this paper.

	X-ray grating	Neutron grating
Grating profiles		
Period, p (nm)	400	2000
Depth, d (nm)	2400	10500
Groove width, w (nm)	180	600
Radiation wavelength (nm)		
Incident angle θ ($^\circ$)	0.1	0.5
SiO ₂ volume percentage in the bulk suspension (%)	90	11.4
Diameter of SiO ₂ particles (nm)	16.7	16.7
Carrier fluid	Dimethylformamide [†]	Deuterated ethanol (45%v) and deuterated benzyl alcohol (55%v)
SLD for silicon (10^{-4} nm^{-2})		
SLD for carrier fluid (10^{-4} nm^{-2})	20.1	2.06
SLD for silica (10^{-4} nm^{-2})	8.33	5.78
SLD for average colloid (10^{-4} nm^{-2})	18.9	3.47
SLD amplitude for structured colloid relative to the average colloid (10^{-4} nm^{-2}) [‡]	10.51	5.39
$\Delta\varphi$: phase through the silicon wall (rad)	1.25	0.22
φ_w : phase through the average colloid (rad)	0.48	5.47
$\bar{\varphi}$: phase through the average colloid (rad)	0.25	14.31
$\Delta\varphi = \bar{\varphi} - \varphi_w$: average phase difference	0.23	8.84
ω_{amp} : phase amplitude generated by structured colloid relative to the average colloid (rad) [‡]	0.03	0.60

[†] Colloids dispersed in various types of carrier fluid were reported by Pfeiffer's group (Bunk *et al.*, 2007; Satapathy *et al.*, 2009; Nygård *et al.*, 2009), including the same one used in neutron experiments (but a mixture of hydrated solvents instead of deuterated solvents) and similar results of colloidal structure were presented. Dimethylformamide is chosen here only because it was used in the X-ray diffraction paper that we are comparing our results with (Nygård *et al.*, 2009). [‡] For the calculation done in this report, we represent the phase modulation in the grating groove by a cosine function (Diaz, 2006). Thus the amplitude of the SLD modulation and the amplitude of the phase modulation refer to the corresponding amplitude of the cosine function. The relationship between the phase amplitude and the SLD amplitude is given by equation (1) in Appendix A.

Fig. 1. The specifications of these gratings, referred to as the X-ray grating and the neutron grating, are defined in Table 1. These values correspond to experiments that have already been carried out and are indicative of values one might expect in future applications.

4. Comparison of the POA and DT analyses

4.1. First approximation in the weak POA method: the constant scaling factor

The first approximation made in the POA analysis is to calculate Bragg intensities for the homogeneously filled grating by applying a constant multiplier to the Bragg intensities measured with an empty grating. However, as shown in Fig. 2(a), this multiplier is not the same for all Bragg orders measured with X-rays. Nevertheless, because the Patterson function involves a sum over Bragg orders and because the first few (intense) Bragg peaks are often well described by the POA, this scaling method yields a good approximation for the

Patterson function of the homogeneously filled grating, as is evident from the small differences between the Patterson functions calculated by DT and by the scaling approach (Fig. 2b).

This, however, does not hold for the neutron experiments. Fig. 2(c) shows the disagreement between the POA and the DT in calculating the ratio between Bragg intensities for the empty and homogeneously filled gratings when using the parameters for the neutron grating shown in Table 1. Note the logarithmic scale used for the ratio in Fig. 2(c). One can clearly see that the POA scaling factor yields very different results for the X-ray and neutron scattering cases. This primarily arises because the neutron grating is much deeper and the angle of incidence is shallower, leading to a phase difference for the empty grating, $\varphi_w = 5.47$ rad, which is much larger than the X-ray value of 0.48 rad. In this case, the POA and the DT give dramatically different results for Bragg intensities, leading to very different Patterson functions, and no constant multiplier can be found that allows the Patterson function of the homogeneously filled grating to be deduced from that of the empty grating. The difference between the Patterson functions for the homogeneously filled grating calculated directly from the DT and that calculated using a constant scaling factor is shown in Fig. 2(d). It is clear from the comparison of Figs. 2(b) and 2(d) that the constant-scaling-factor approach is not adequate for the neutron case, whereas it is a justified approximation for the X-ray case as in the experiments reported by Nygård *et al.* (2009).

4.2. Second approximation: the weak phase approximation

The X-ray analysis method assumes that the change in scattering due to colloidal structure results from a small phase change that can be treated as a perturbation. This means that even if the Bragg intensities for the homogeneously filled grating were known exactly, it is understood that we might not be able to retrieve the phase modulation resulting from colloid structure using the X-ray analysis if the modulation amplitude is too large. However, the development of the perturbation theory imposes no constraint on the average phase, $\bar{\Delta\varphi}$, even though the Patterson function is only equal to the autocorrelation function of the transmission function for weak scattering. For large values of $\bar{\Delta\varphi}$, the experimental data do not directly yield the autocorrelation function, which is a condition for the perturbation analysis to be applicable.

Our calculations for various grating specifications and different colloidal structures in the grating grooves show that, even if the phase modulation caused by colloidal structure is small, the X-ray holography method may still fail to give a correct result when the average phase difference, $\bar{\Delta\varphi}$, between the grating channels and walls is large. In fact, empirically, we find that $\bar{\Delta\varphi}$ has to be less than about π radians for the weak phase method to work, even if the phase modulation due to colloidal structure is small and if the Patterson function of the homogeneously filled grating could be known exactly.

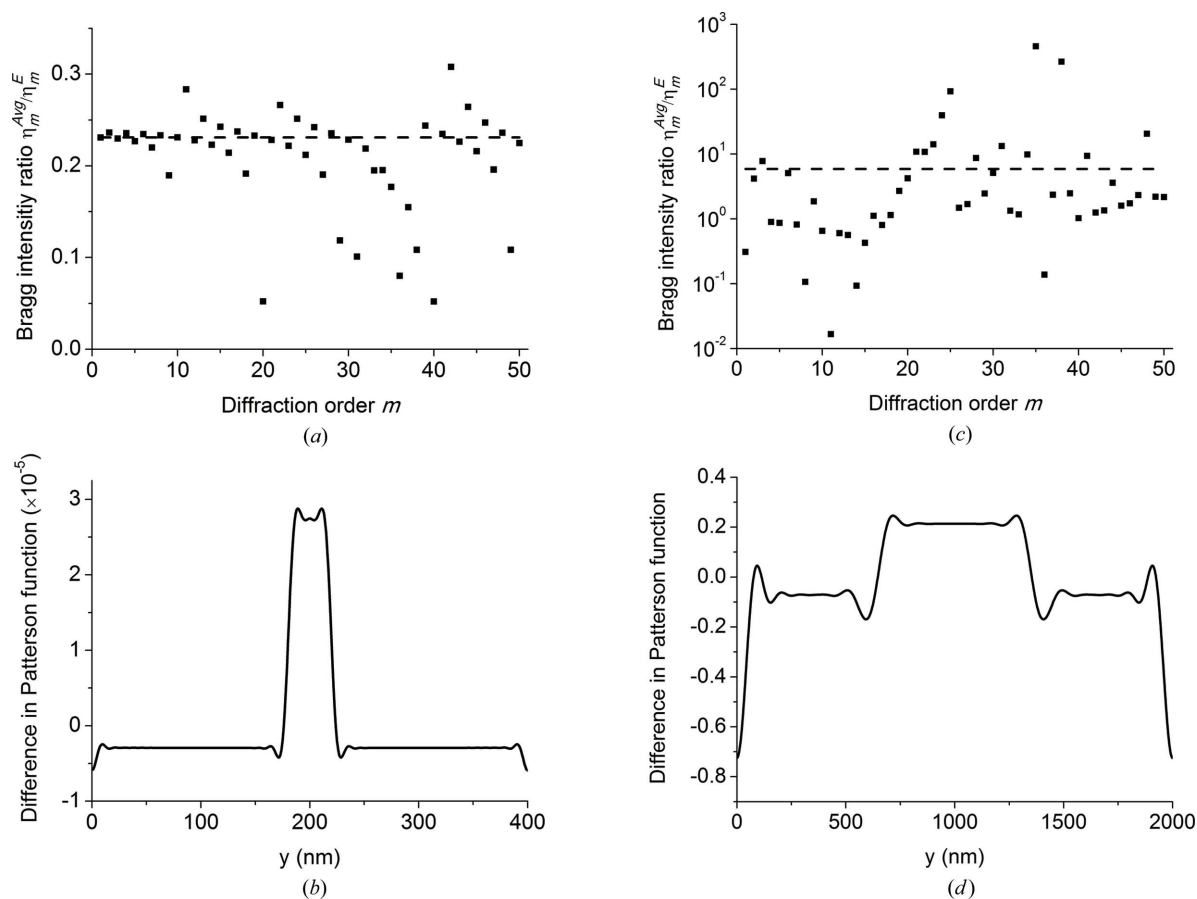


Figure 2 (a) Calculated ratios for non-zero-order Bragg peaks for a homogeneously filled grating and an empty grating using the parameters of the X-ray grating. The dots denote the DT calculation while the flat dashed line is calculated using the POA. (b) Difference between the Patterson functions calculated using DT for a homogeneously filled X-ray grating and the function calculated by the scaling Bragg intensities for an empty X-ray grating using a constant scaling factor. Panels (c) and (d) are the plots for the neutron experiment corresponding to (a) and (b), respectively.

4.3. Investigating the validity of the weak POA method based on two grating profiles in the X-ray and SESANS experiments

Fig. 3 shows the results that would be obtained in typical X-ray and neutron experiments analyzed using the weak POA. Parts (a) and (e) of Fig. 3 represent the SLD profiles of a putative structured colloid and the corresponding average colloid for the X-ray and neutron experiments, respectively. The two-layer SLD profile in Fig. 3(a) is similar to the profile obtained by Nygård *et al.* (2009): there are two complete layers of colloidal particles in the grooves, parallel to the groove walls. Since Nygård *et al.* (2009) reported almost no increase in particle density in the grooves (17.2% average in the grooves *versus* 16.7% in the bulk), we use an average volume fraction of silica particles of 16.7% in the grating grooves. The experimental results obtained by Nygård *et al.* (2009) indicate an SLD contrast modulation relative to the average that can be captured by a cosine function. The modulation used in both the X-ray and the neutron cases is similar in magnitude to what one would expect on the basis of the structure deduced from the X-ray experiment. DT calculations of the Bragg intensities for the average and structured colloid result in the Patterson functions shown in Fig. 3(b). The difference between the two Patterson functions (Fig. 3c) shows two dips

between $y = 0$ nm and $y = 180$ nm, at $y = 30$ nm and $y = 116$ nm, indicative of two colloidal layers separated by about 84 nm. Fig. 3(d) shows the extracted phase profile obtained using the deconvolution equation [equation (13) in Appendix A]. The fact that the result is very close to the phase modulation input into the calculation demonstrates that the method developed by Nygård *et al.* (2009) works well for the X-ray case considered here, even if it does predict unphysical phase modulation outside the region of the grooves.

Parts (e), (f), (g) and (h) in Fig. 3 are the corresponding plots using the parameters for an analogous neutron experiment. If we employ the same volume fraction of silica particles used in the X-ray experiments (16.7%), the SLD of a putative structured colloid, the appropriate average colloid and the carrier fluid (45% deuterated ethanol and 55% deuterated benzyl alcohol) would have the profiles shown in Fig. 3(e). The SLD contrast modulation, the cosine function with amplitude $0.22 \times 10^{-4} \text{ nm}^{-2}$, corresponds to a potential close-packed structure in each layer, similar to the one deduced from the X-ray experiment. Figs. 3(f) and 3(g) show the corresponding Patterson functions and their difference, respectively. Compared with the X-ray case (Fig. 3c), the calculations for the neutron scenario show more pronounced discrepancies

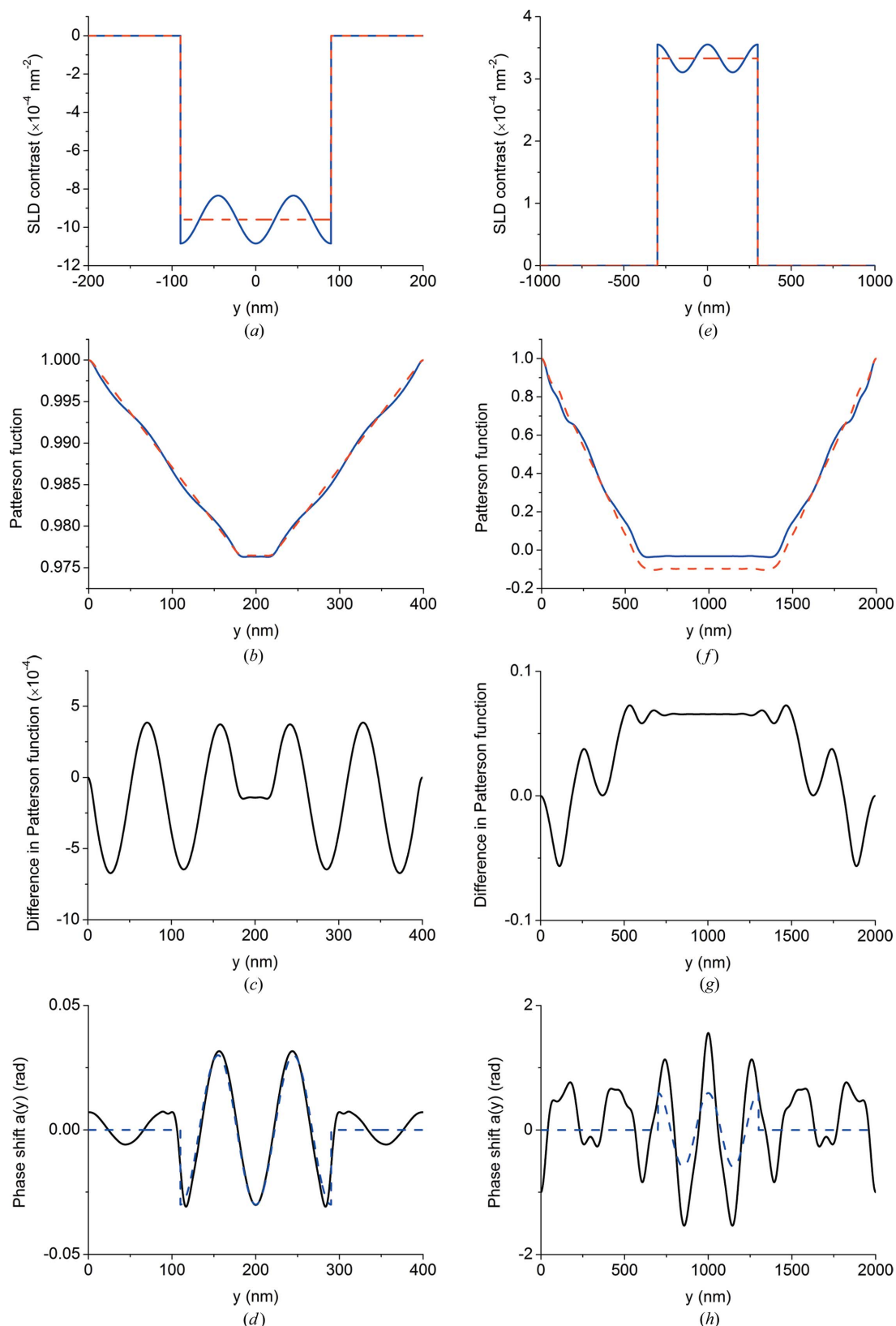


Figure 3

(a) The X-ray SLD contrast with respect to the silicon walls of a grating with a two-layer structured colloid (solid line) and the corresponding average colloid (dashed line). (b) DT calculations of the Patterson functions using the SLD profiles in panel (a) for a grating with a two-layer structured colloid (solid line) and a homogeneously filled grating (dashed line). (c) The difference between the two Patterson functions shown in panel (b). (d) Calculated phase profile across the grating in the y direction. The solid line denotes the phase profile determined from the difference function plotted in panel (c), while the dashed line is the phase profile input (cf. Fig. 3a). Panels (e), (f), (g) and (h) are the analogs of (a), (b), (c) and (d) calculated using the parameters for the neutron experiment listed in Table 1.

between the Patterson functions of the average and structured colloid. The comparison of the phase modulation input and that deduced using the deconvolution method described here (Fig. 3*h*) clearly shows that the deconvolution method is not adequate for phase retrieval in the neutron measurements. We also note that the fact that the number of phase oscillations in the grooves is correctly reproduced in this case is mere chance: it can be completely different for gratings with a slightly different average phase $\overline{\Delta\varphi}$.

5. Summary and conclusions

Even though modern silicon gratings can now be manufactured with rectangular profiles that are deep and almost perfect (Diaz *et al.*, 2005; David *et al.*, 2007), there is almost always some degree of trapezoidal shape to their profiles. For a trapezoidal grating, the theoretical underpinnings of the weak POA method are undermined. The existence of a constant ratio between the Bragg intensities of the empty and homogeneously filled gratings depends either on the applicability of equation (2) in Appendix A, which is true only for a rectangular grating, or on the validity of a lowest-order expansion of $\exp[i\overline{\Delta\varphi}f(y)]$, where $f(y)$ is no longer a simple step function. If the inclination angle of the grating wall is not too large and the phase contrast is small, the calculated ratios between the Bragg intensities of empty and homogeneously filled gratings is still almost constant. This is true for calculations done with either the POA or the DT, although the actual values of the ratios differ. If the phase difference is large, either for the empty grating or for the homogeneously filled grating, even a slightly inclined grating wall leads to calculated Bragg ratios that differ remarkably from the value calculated for a rectangular grating. This is true both for the POA and for the DT.

The problem that this raises is obvious: how does one find a value for the constant multiplier that is sufficiently accurate that it does not jeopardize the integrity of data analysis based on the weak phase approximation? While some rules of thumb have emerged from our simulations, there appears to be no simple answer to this question. For empty or homogeneously filled gratings with a phase contrast less than about π , we empirically find that the weak POA method works for many cases provided the colloid only produces a weak phase modulation. For phase contrasts greater than π , the conventional POA and the DT predict increasingly different Patterson functions. The differences are especially large for square gratings when the phase modulations are around 2π , where the POA predicts no scattering at all. Since the conventional POA is the basis for expecting a constant ratio between Bragg intensities of the empty and homogeneously filled grating, we might expect the ratio to differ from a constant when the POA itself breaks down, and indeed this is what we see in our calculations. For gratings with trapezoidal profiles, this is also true. The necessary but not sufficient condition for calculating the Patterson function for the homogeneously filled grating from that of the empty grating by multiplying a constant number is that the two should at

least have a similar shape. However, by doing calculations using either the conventional POA or the DT for trapezoidal gratings, we find that the shape of the Patterson functions changes significantly as the phase contrast increases.

Since the relative error in the modulation profile retrieved from the weak POA method is $O(\omega_{\text{amp}})$, one would expect the method to fail eventually when ω_{amp} is large. In such a scenario, one can no longer use the weak POA method to deduce the colloidal structure in a grating and one has to use either the conventional POA or the DT, making data analysis much more involved.

APPENDIX A

For a periodic rectangular grating, the phase difference between waves passing through a groove and a wall can be expressed as

$$\Delta\varphi = \Delta\rho\lambda h/\sin\theta, \quad (1)$$

where $\Delta\rho$ represents either the X-ray or neutron SLD contrast between the grating and the medium in the grooves; λ is the radiation wavelength; h is the depth of grating grooves and θ is the incident angle (see Fig. 1). Since all gratings analyzed in this paper are translationally invariant in the x direction, scattering from the grating will not change the x component of the wavevector so we need only consider scattering in the yz plane. Assuming the grating to be non-absorbing, the transmission function of the colloids in the grating calculated from the POA approach of Nygård *et al.* (2009) is

$$t^C(y) = \exp[i\Delta\varphi(y)] = 1 + (\exp\{i[\overline{\Delta\varphi} + \omega(y)]\} - 1)f(y). \quad (2)$$

For grating holography, the phase change caused by material in the grating grooves can be divided into two parts: the phase change caused by an average colloid, $\overline{\Delta\varphi}$, and a part that represents the deviation of the colloidal structure from this average value, $\omega(y)$. Such deviations cause a small change in the overall radiation phase so that in the weak phase approximation equation (2) can be expanded to lowest order:

$$t^C(y) \simeq 1 + [\exp(i\overline{\Delta\varphi}) - 1]f(y) + i\omega(y)f(y)\exp(i\overline{\Delta\varphi}). \quad (3)$$

Within the POA, the intensity of the m th Bragg peak is equal to the squared modulus of the m th Fourier coefficient of the transmission function given in equation (2):

$$\eta_m^C = |T_m^C|^2. \quad (4)$$

Here, η_m^C is the m th-order Bragg intensity for the grating in the colloidal suspension and T_m^C is the appropriate m th-order Fourier coefficient of the transmission function, *i.e.*

$$T_m^C \simeq \delta_{0,m} + [\exp(i\overline{\Delta\varphi}) - 1]F_m + iA_m \exp(i\overline{\Delta\varphi}), \quad (5)$$

$$T_m^{\text{Avg}} = \delta_{0,m} + [\exp(i\overline{\Delta\varphi}) - 1]F_m, \quad (6)$$

with T_m^C , F_m and A_m standing for the coefficients in the Fourier expansions of $t^C(y)$, $f(y)$ and $a(y) = \omega(y)f(y)$. If we can

combine equations (4), (5) and (6), the non-zeroth-order Bragg intensities for the case of the grating in the colloidal suspension can be approximated as

$$\eta_m^C \simeq \eta_m^{\text{Avg}} + 2A_m F_m \sin \overline{\Delta\varphi} + A_m^2. \quad (7)$$

In the weak phase approximation, the quadratic term A_m^2 is small and can be neglected. The Bragg intensities are linked to the one-dimensional Patterson function and the autocorrelation function (ACF) as follows (Diaz, 2006):

$$\text{ACF} \equiv \frac{1}{p} t^C(y) \otimes t^{C*}(-y) = \sum_{-\infty}^{\infty} \eta_m^C \cos\left(\frac{2\pi my}{p}\right) \equiv P^C(y). \quad (8)$$

The difference between the Patterson functions for the structured colloid and the homogeneously filled grating is given by

$$\Delta P(y) = P^C(y) - P^{\text{Avg}}(y). \quad (9)$$

Combining equations (7), (8) and (9) with A_m^2 omitted, we get

$$\begin{aligned} \Delta P(y) &= \sum_{-\infty}^{\infty} (\eta_m^C - \eta_m^{\text{Avg}}) \cos\left(\frac{2\pi my}{p}\right) \\ &\simeq \left(\frac{2 \sin \overline{\Delta\varphi}}{p}\right) a(y) \otimes f(y). \end{aligned} \quad (10)$$

The X-ray experiment measures η_m^C directly, but before we can obtain the phase-shift profile $a(y)$ from equation (10), we need the value of η_m^{Avg} for all m . Since η_m^{Avg} represents the m th-order Bragg intensity for the homogeneously filled grating, it cannot be determined experimentally. Nevertheless, within the POA, these Bragg intensities can be calculated from the corresponding Bragg intensities for the empty grating, which are experimentally obtainable. For nonzero diffraction orders

$$\frac{\eta_m^{\text{Avg}}}{\eta_m^E} = \frac{|\exp(i\overline{\Delta\varphi}) - 1| F_m|^2}{|\exp(i\varphi^E) - 1| F_m|^2} = \frac{\sin^2(\overline{\Delta\varphi}/2)}{\sin^2(\varphi^E/2)} \equiv S, \quad (11)$$

with φ^E representing the phase difference for an empty grating and S being a constant that is independent of the index m . For a weak phase object where $\overline{\Delta\varphi}$ and φ^E are small, the above relation reduces to $\eta_m^{\text{Avg}}/\eta_m^E \propto (\overline{\Delta\varphi}/\varphi^E)^2$, as obtained within the kinematic approximation. In the approximation where the zeroth diffraction order and the total scattering are negligibly affected by the ordering of fluid in the groove, we have $\eta_0^{\text{Avg}} \simeq \eta_0^C$ and $\sum_{m \neq 0} \eta_m^{\text{Avg}} \simeq \sum_{m \neq 0} \eta_m^C$, so S can be calculated from the experimentally measured quantities as

$$S = \frac{\sum_{m \neq 0} \eta_m^{\text{Avg}}}{\sum_{m \neq 0} \eta_m^E} \simeq \frac{\sum_{m \neq 0} \eta_m^C}{\sum_{m \neq 0} \eta_m^E}. \quad (12)$$

With equations (10), (11) and (12), one can calculate $\Delta P(y)$. Finally, $a(y)$ can be determined by deconvoluting from $\Delta P(y)$ using the known window function $f(y)$:

$$a(y) = \frac{1}{2 \sin \overline{\Delta\varphi}} \sum_{-\infty}^{\infty} \frac{\int_{-p/2}^{p/2} \Delta P(y) \cos(-2\pi my/p) dy}{\int_{-p/2}^{p/2} f(y) \cos(-2\pi my/p) dy} \cos\left(\frac{2\pi my}{p}\right). \quad (13)$$

Acknowledgements

RP is grateful to the University of California at Santa Barbara MRSEC for the use of their facilities during the preparation of this manuscript. Fabrication of the neutron grating was conducted at the Center for Nanophase Materials Sciences, which is a DOE Office of Science User Facility.

Funding information

This work was supported by the US Department of Energy through its Office of Basic Energy Sciences, Division of Material Science and Engineering (grant No. DE-FG02-09ER46279). The UCSB MRSEC is supported by the National Science Foundation, Division of Materials Research, through grant No. 1121053. RA acknowledges support from the Clifford G. Shull Fellowship program at Oak Ridge National Laboratory.

References

- Ashkar, R., de Haan, V. O., van Well, A. A., Dalgliesh, R., Plomp, J., Fitzsimmons, M. R., Schaich, W. L. & Pynn, R. (2011). *J. Appl. Cryst.* **44**, 958–965.
- Ashkar, R., Pynn, R., Dalgliesh, R., Lavrik, N. V. & Kravchenko, I. I. (2014). *J. Appl. Cryst.* **47**, 1367–1373.
- Ashkar, R., Stonaha, P., Washington, A. L., Shah, V. R., Fitzsimmons, M. R., Maranville, B., Majkrzak, C. F., Lee, W. T., Schaich, W. L. & Pynn, R. (2010). *J. Appl. Cryst.* **43**, 455–465.
- Bunk, O., Diaz, A., Pfeiffer, F., David, C., Padeste, C., Keymeulen, H., Willmott, P. R., Patterson, B. D., Schmitt, B., Satapathy, D. K., van der Veen, J. F., Guo, H. & Wegdam, G. H. (2007). *Phys. Rev. E*, **75**, 021501.
- David, C., Bruder, J., Rohbeck, T., Grünzweig, C., Kottler, C., Diaz, A., Bunk, O. & Pfeiffer, F. (2007). *Microelectron. Eng.* **84**, 1172–1177.
- Daw, R. & Finkelstein, J. (2006). *Nature*, **442**, 367–418.
- Diaz, A. (2006). PhD thesis, Paul Scherrer Institute, Switzerland.
- Diaz, A., David, C., Guo, H., Keymeulen, H., Pfeiffer, F., Wegdam, G., Weitkamp, T. & van der Veen, J. (2005). *Physica B*, **357**, 199–203.
- Diaz, A. & van der Veen, J. (2007). *Thin Solid Films*, **515**, 5645–5653.
- Gähler, R., Golub, R., Habicht, K., Keller, T. & Felber, J. (1996). *Physica B*, **229**, 1–17.
- Haan, V.-O. de, Plomp, J., Bouwman, W. G., Trinker, M., Rekveldt, M. T., Duif, C. P., Jericha, E., Rauch, H. & van Well, A. A. (2007). *J. Appl. Cryst.* **40**, 151–157.
- Jap, B. K. & Glaeser, R. M. (1978). *Acta Cryst.* **A34**, 94–102.
- Krouglov, T., de Schepper, I. M., Bouwman, W. G. & Rekveldt, M. T. (2003). *J. Appl. Cryst.* **36**, 117–124.
- Nygård, K., Satapathy, D., Bunk, O., Diaz, A., Perret, E., Buitenhuis, J., Pfeiffer, F., David, C. & van der Veen, J. (2008). *Opt. Express*, **16**, 20522–20529.
- Nygård, K., Satapathy, D. K., Bunk, O., Perret, E., Buitenhuis, J., David, C. & van der Veen, J. F. (2009). *J. Appl. Cryst.* **42**, 1129–1138.
- Rekveldt, M. T. (1996). *Nucl. Instrum. Methods Phys. Res. B*, **114**, 366–370.
- Rekveldt, M. T., Plomp, J., Bouwman, W. G., Kraan, W. H., Grigoriev, S. & Blaauw, M. (2005). *Rev. Sci. Instrum.* **76**, 033901.
- Satapathy, D., Nygård, K., Bunk, O., Jefimovs, K., Perret, E., Diaz, A., Pfeiffer, F., David, C. & van der Veen, J. (2009). *Europhys. Lett.* **87**, 34001.
- Windbergs, M. & Weitz, D. A. (2011). *Small*, **7**, 3011–3015.